NRL Memorandum Report 4826

An Experimental Study of the Hydrodynamics of Reduced Density Channels

J. R. GREIG, R. E. PECHACEK, M. RALEIGH, AND K. A. GERBER

Plasma Physics Division

June 10, 1982

NAVAL RESEARCH LABORATORY
Washington, D.C.

SECURITY CLASSIFICATION OF THIS PAGE (When Data Entered)

REPORT DOCUMENTATION PAGE

READ INSTRUCTIONS BEFORE COMPLETING FORM

1. REPORT NUMBER: NRL Memorandum Report 4826	2. GOVT ACCESSION NO.: AD-A116408
3. RECIPIENT'S CATALOG NUMBER	
4. TITLE (and Subtitle): AN EXPERIMENTAL STUDY OF THE HYDRODYNAMICS OF REDUCED DENSITY CHANNELS	5. TYPE OF REPORT & PERIOD COVERED: Interim report on a continuing problem
	6. PERFORMING ORG. REPORT NUMBER
7. AUTHOR(s): J. R. Greig, R. E. Pechacek, M. Raleigh, and K. A. Gerber	8. CONTRACT OR GRANT NUMBER(s)
9. PERFORMING ORGANIZATION NAME AND ADDRESS: Naval Research Laboratory, Washington, DC 20375	10. PROGRAM ELEMENT, PROJECT, TASK AREA & WORK UNIT NUMBERS: 61153N;R011-09-41;47-0871-0-2; and 62707E;0;OR40AA
11. CONTROLLING OFFICE NAME AND ADDRESS: Office of Naval Research, Arlington, VA 22217; Defense Advanced Research Projects Agency, Arlington, VA 22209 ATTN: Program Management/MIS	12. REPORT DATE: June 10, 1982
	13. NUMBER OF PAGES: 32
14. MONITORING AGENCY NAME & ADDRESS(if different from Controlling Office): Naval Surface Weapons Center, White Oak, MD 20910 ATTN: R-401	15. SECURITY CLASS. (of this report): Unclassified
	15a. DECLASSIFICATION/DOWNGRADING SCHEDULE

16. DISTRIBUTION STATEMENT (of this Report)

Approved for public release, distribution unlimited

17. DISTRIBUTION STATEMENT (of the abstract entered in Block 20, if different from Report)

18. SUPPLEMENTARY NOTES

Research supported by the Office of Naval Research and by the Defense Advanced Research Projects Agency (DoD) ARPA Order No. 4395 monitored by the Naval Surface Weapons Center under Contract N60921-82-WR-W0066.

19. KEY WORDS (Continue on reverse side if necessary and identify by block number)

Reduced Density Channel
Hydrodynamics
Turbulence
Cooling

20. ABSTRACT (Continue on reverse side if necessary and identify by block number)

Experiments on both the formation and decay of reduced density channels in gaseous atmospheres have been performed using a novel method to produce channels in nitrogen by the absorption of pulsed CO_2 laser radiation. These experiments were performed in a chamber consisting of three regions: a nonabsorbing convergence section filled with pure nitrogen in which the CO_2 laser beam was focused to small diameter and high intensity; a windowless transition region; and an absorption section filled with nitrogen containing a small percentage of SF_6. The amount of laser energy absorbed in the gas ($\gtrsim 0.4$ J/cm^3) and the radius of the laser beam ($\sim$2 mm) were measured (Continued)

DD FORM 1 JAN 73 1473 EDITION OF 1 NOV 65 IS OBSOLETE
S/N 0102-014-6601

SECURITY CLASSIFICATION OF THIS PAGE (When Data Entered)

20. ABSTRACT (Continued)

throughout the absorption section. The radial density profile of the resulting channel was determined as a function of time by several optical methods.

Hydrocode simulations of the evolution of the radial density profile of the channel were performed based on the measured initial conditions and agree well with the measured results for the first ~100 μs of the life of the channel. At later times these channels have been observed to dissipate rapidly (~10^3 faster than thermal conduction) due to turbulent mixing. A recent theory, due to Boris and Picone, concerning the source of this turbulence is discussed and the results of further experiments which tend to confirm this theory are reported.

Measurements of the rate of channel dissipation are presented and it is shown that the mixing effect of turbulence can be represented by a diffusive model in which the anomolous diffusivity is 10^2 to 10^3 times larger than that caused by thermal conduction.

100 to 1000

about 1000

about 100 microseconds

CONTENTS

AN EXPERIMENTAL STUDY OF THE HYDRODYNAMICS OF REDUCED DENSITY CHANNELS

I. INTRODUCTION

We report the results of studies of the hydrodynamics of hot, reduced density channels produced by focusing a pulsed CO_2 laser[1] in 900 torr of nitrogen containing 0.7% SF_6 as an absorbant. We also describe the hardware developed to perform these experiments.

These channels were studied to determine the mechanisms which control the cooling of hot channels in the atmosphere and the rate at which such channels cool. Observations of the channel formation are compared with results from the 1-D hydrocode, ETBFCT which predicts the relationship of radial heating profiles to the evolution of the channel density profile.[2] Observations of the channel decay are compared to results taken from recently developed theories[3] and computations which allow asymmetries in the channel profile to induce vorticity and thus to enhance channel cooling by convective mixing. To create specific asymmetries, channels were produced using multiple heating (laser) pulses which could be separated spatially and/or temporally.

Channel cooling is of particular interest for the case of lightning channels in the atmosphere, where it has been suggested[4] that significantly enhanced cooling rates, i.e., much larger than caused by thermal conduction, are necessary to explain the production of oxides of nitrogen in the atmosphere. In similar experiments using the channels produced by laser-guided and unguided, electric discharges in the atmosphere[5] we have already shown that such channels cool by convective mixing and that the cooling rate is $\sim 10^3$ times that anticipated from thermal conduction. The difference in the experiments reported here is that for the CO_2 laser produced channels the amount of energy deposited was less than for the electric discharges ($\sim$0.1 J/cm compared with $\sim$3 J/cm); the energy was deposited more uniformly across the channel diameter; and the geometric perturbations (kinks and bends) imposed during channel formation were much smaller.

II. EXPERIMENTAL APPARATUS

i. Description of the Chamber

The chamber consists of an aluminum cylinder 3.5 m long and .3 m inner diameter: it is shown in Fig. 1. The CO_2 laser beam entered the 2.5 m long convergence section through a 23 cm diameter, 3 m focal length NaCl lens (a), passed through a short transition region consisting of two baffles (b,c) 6.5 cm apart having 7.5 cm diameter holes in their centers, and entered the 1 m long absorption section. Windows (d) 15 cm in diameter, allowed both horizontal and vertical lines of sight through the center of the absorption section. A NaCl window (e) in the end of this section permitted external monitoring of the transmitted CO_2 laser beam. Horizontal pairs of 2.5 cm ports (f) are part of the gas composition monitoring system described in section iii.

Nitrogen entered the convergence section at (g) and SF_6 doped nitrogen entered the absorption section at (h). The nitrogen had to exit the convergence section through the baffle at (b). Thereafter, the combined gases left the chamber through exhaust ports at either (i) or (j). A mechanical vacuum pump (k) was provided to evacuate the chamber after each shot.

Manuscript submitted, March 18, 1982.

The pure nitrogen for the convergence section was supplied from a regulated cylinder through a metering valve and a flow gauge. The mixture for the absorption section was supplied by mixing metered flows of SF_6 and nitrogen, from regulated cylinders, in a mixing manifold.

ii. Operating Procedure

The chamber was initially evacuated to a pressure of 200 m Torr. All sections were then filled to just above 1 atm with pure nitrogen. At this time the exhaust valves were opened and nitrogen flow rates of 21 l/min and 12 l/min in the convergence and absorption sections were set. One minute was allowed to establish a steady state flow condition in which the chamber pressure stabilized at 900 Torr. SF_6 was then added to the nitrogen flow in the mixing manifold and a 15 minute purging of the absorption section was allowed prior to a shot. (These gas handling procedures were initially tested using brown N_2O_4 in place of the SF_6 to allow the flow patterns to be observed.)

High intensity 10.6 μ radiation is strongly absorbed by the vibrational structure of the SF_6 molecule in a nonlinear multiphoton process.[6,7] The energy is collisionally transferred into heat of the nitrogen gas. The collisional transfer rate for vibrational-translational relaxation is the limiting step in the process and saturable absorption occurs at modest laser intensities. However at the very high laser intensities used in these experiments multiphoton absorption takes place and a much faster energy transfer ensues[7] (see Section III, i). This absorptive property was demonstrated by the ability of a small percentage of SF_6 to suppress the aerosol-induced breakdowns that occurred when full CO_2 laser energy reached the minimum beam waist as shown in Fig. 2. The figure shows schlieren photographs taken 4 μsec after the CO_2 laser pulse with differing concentrations of SF_6. The photographs were taken through the 15 cm windows (d) in the absorption section.

iii. SF_6 Monitoring System

The concentration of SF_6 at various positions in the chamber was monitored by measuring the absorption of low power cw CO_2 laser beams directed across the chamber diameter. This system is shown in Fig. 3. The beam from a horizontally polarized 3 w CO_2 laser was directed through a series of three adjustable-output beam splitters. Each beam splitter redirected a small fraction of the laser beam through a ZnSe window, across the chamber, and into a pyroelectric detector. A window and a detector were mounted in each pair of 2.5 cm ports (f). Milli-voltmeters monitored the output of each detector. The voltage readings of the detectors in the convergence section did not normally drop during the 15 minute gas flow operation. However the output of the detector in the absorption section fell to zero in a few minutes.

The adjustable-output beam splitter, shown in Fig. 4, re-directs a fraction of the CO_2 laser beam at a constant 90° deviation and without change in lateral position. The horizontally polarized input beam is incident at angles near Brewsters angle on a ZnSe beam splitter (a). The reflected beam strikes a totally reflecting mirror (b) completing the 90° deflection. Both the splitter and the mirror are vertically mounted on a horizontal rotary table. The line of intersection of their faces coincides with the axis of rotation. Rotating the table varies the output beam intensity but not its deviation or position. The bulk of the incident beam is transmitted without deviation but with a variable lateral displacement. Therefore the monitoring system was aligned starting with the splitter nearest the cw CO_2 laser.

iv. Diagnostics

The channel was normally un-ionized and nonluminous. Breakdowns due to insufficient SF_6 and/or excessive CO_2 laser energy were observed through the 15 cm windows using open shutter cameras.

The total laser power incident on the NaCl lens was measured with a large, full beam calorimeter and simultaneously with a calorimeter/beam splitter sampling ~10% of the full beam energy. The sampling calorimeter was thus calibrated to give the total incident power and remained in the laser beam(s) on all shots. A photon drag detector also received a portion of the sampled beam to give timing references.

A small, volume absorbing calorimeter was constructed by embedding Cr-Al thermocouples in polyethylene. This calorimeter was mounted on a telescoping stalk attached on axis to the end plate of the chamber and was used to measure laser energy as a function of axial distance within the absorbing section. A similar stalk was used to hold burn paper to measure beam profiles. The paper has a measured minimum threshold of .5 J/cm^2 and a saturation limit of 2.5 J/cm^2.

Four different optical systems were used to detect the channels through the refractive index changes caused by the neutral gas density variations. All these systems looked through the 15 cm windows (d) on the absorption section. Qualitative pictures of the channels were taken using a schlieren system which followed normal practice except for the substitution of a 1 mm pinhole for the usual knife-edge. This reduces the sensitivity of the system but allows it to detect density gradients in all directions rather than just perpendicular to the knife-edge. When the schlieren system was illuminated by a pulsed ruby laser (~25 ns FWHM) the channel motion at early times (~0 to 50 μs after the CO_2 laser pulse) was stopped. Late time behavior was observed by illuminating the schlieren system with a cw HeNe laser and recording the output with a high speed 16 mm movie camera. The camera took a 40 μs exposure every 100 μs which was sufficiently rapid to stop hydrodynamic motion that occurred after the initial channel expansion phases were over. Shock waves were seen as blurs on the movie frames.

A quantitative schlieren system was used to measure radial density profiles.[8] The system (Fig. 5) directed a vertical ribbon of light across the channel. Vertical deflections of this light due to the reduced density channel and the shock wave appear as horizontal deflections of the ribbon when it is imaged onto the film. The result is therefore a plot of angular deflection versus impact parameter and may be inverted to yield the channel density profile. This system was used at both early and late times and was illuminated by the pulsed ruby laser.

Radial density profiles at early times were also measured via double-exposure holographic interferometry using the pulsed ruby laser. The methods suggested by Jahoda and Siemon[9] were used with the channel imaged onto the holographic plate to allow a white light playback system.

A large Mach-Zehnder interferometer, with 6 inch diameter optics, was used to take interferometric movies of the late time channel behavior using the same HeNe laser and high speed camera as used for the schlieren movies.

v. Shock Attenuation

Formation of the reduced density channel created an outwardly expanding cylindrical shock wave. This wave was reflected from the aluminum chamber wall and refocused on the channel. The returning shock may have influenced the hydrodynamic behavior of the channel and had therefore to be attenuated. Figure 6(a) is a quantitative schlieren photograph showing the unattenuated returning shock. The characteristic pulse width behind the shock front is ~.5 cm. Therefore the chamber was lined with carpeting having a ~.5 cm pile depth and spacing between ridges. Figure 6(b) shows the improvement caused by carpeting the chamber.

III. CHANNEL EVOLUTION

i. The Absorption Mechanism

The CO_2 laser pulses consisted of a $\sim$100 ns spike containing $\sim$16 J followed by a $\sim$2 μs tail containing $\sim$32 J. At focus the resultant fluxes were $\sim 5 \times 10^8$ w/cm^2 in the spike and $\sim 2.5 \times 10^7$ w/cm^2 in the tail. At these fluxes the SF_6 molecules were multiply excited and vibrational-translational energy transfer was greatly enhanced.[7] At low laser intensity the collision cross-section for energy transfer is

$$\sigma_{V\text{-}T} \sim 10^{-17} \text{ cm}^2$$

and rises to

$$\sigma^*_{V\text{-}T} \sim 10^{-16} \text{ cm}^2$$

at high intensity while the absorption cross-section for 10.6 μm radiation in SF_6 is[6]

$$\sigma_A \sim 10^{-17} \text{ cm}^2.$$

Thus the rate of population of the "excited" SF_6 levels may be approximated by

$$\frac{dn^*}{dt} \sim n_a \sigma_A \phi - n^* \{\sigma_A \phi + \sigma_{V\text{-}T}\, n_3 v\}$$

where n^*, n_a, and n_3 are the populations of the excited SF_6 state, the total SF_6 population, and total gas population (N_2 + SF_6) respectively, ϕ is the laser photon flux, and v the mean thermal velocity. For the above laser fluxes and the quoted ground state absorption cross-section the equilibration time for the excited state population was always much less than the relevant irradiation time. Therefore we conclude that the SF_6 molecules spent most of their time in the excited state. In reality the SF_6 molecules were multiply excited to levels in the near-continuum of excited states[10] known to exist in SF_6. The excited molecules did not return to the ground state following an inelastic collision but only dropped to some lower excited state. Thus σ_A decreased to that of the lower excited state and we suspect that the SF_6 molecules were continuously cycled between the upper and lower excited states. Then the net energy transfer to kinetic energy of the gas was

$$\frac{d E_{\text{kinetic}}}{dt} \sim \frac{1}{2}\, n_a\, \sigma^*_{V\text{-}T}\, v\, n_3 h\nu$$

which when "integrated" over the CO_2 laser pulse was $\sim$.4 J/cm^3 in the target zone where the concentration of SF_6 molecules was $\sim 2.0 \times 10^{17}$ cm^{-3}. The rate of energy absorption was therefore limited by the concentration of SF_6 but may have increased beyond .4 J/cm^3 as v rose.

Absorption Measurements

The laser energy per pulse, incident on the salt lens was normally $\sim$50 J. Measurements were also made inside the absorption section of the experimental chamber of the surviving laser energy as a function of the distance from the lens. These measurements were made under actual gas flow conditions. The calorimeter used in these measurements could not be placed within the transition section of the chamber but extrapolation of the data shows the entire 50 J was being transmitted through the clean nitrogen in the convergence section. The energy absorbed per unit length was derived from these measurements (Fig. 7). Values of $\sim$0.15 J/cm and $\sim$0.05 J/cm were measured at the "upstream" and the "downstream" sides respectively of the field of view through the 15 cm windows. Beam burn patterns were also taken, as a function of distance from the lens, under actual gas flow conditions. The energy deposition per unit volume was derived from the calorimeter and burn pattern measurements. The absorption appears to saturate in the forward end of the absorption section at $\gtrsim$.6 J/cm^3 and to fall for the remaining distance away from the lens. A value of $\gtrsim$.4 J/cm^3 appears characteristic of the channel segment seen through the 15 cm windows. These measurements thus agree with the predicted saturation limit.

iii. Energy Deposition Radius

The best direct evidence of the effective radius of the laser beam, i.e., the radius over which energy is absorbed, comes from quantitative schlieren photographs of the channel at early times (Fig. 8). The pattern of spikes seen in Fig. 8 corresponds to an outward going shock which was just forming and an inward going rarefaction which had yet to reach the axis. These two waves started near the edge of the laser beam and propagated away from each other. The shock was supersonic while the rarefaction was sonic within a hot medium. Assuming similar speeds for both waves and measuring the appropriate spacing on the photograph yields an estimate of the initial radius as $\sim$2.5 mm. This agrees well with the radius of $\sim$2.5 mm that one infers from the burn patterns (Fig. 9).

iv. Basic Experimental Observations

The first observations of a single CO_2 laser pulse interacting with the doped gas were made with the open shutter camera and the schlieren system illuminated by the pulsed (25 ns) ruby laser. At low SF_6 concentrations luminous breakdowns were seen by the still camera and spherical disturbances by the schlieren system (Fig. 2). When the SF_6 concentration was increased to $\sim$0.7% by volume these phenomena were suppressed and a reproduceable cylindrical channel resulted which was invisible to the still camera but could be seen by the schlieren system (Fig. 10a). The channel assumed a fluted appearance after $\sim$250 μs and after $\sim$900 μs acquired a chaotic, turbulent structure. These changes were accompanied by a growth in the average channel size. The channel density gradients eventually became too weak to be detected by the schlieren system after $\sim$10 ms.

Subsequently the channels were observed using holographic interferometry and quantitative schlieren photography, both with the pulsed ruby laser (25 ns) as the light source. These techniques permitted a detailed study of the evolution of the channel at early times. Typical interferograms are shown in Fig. 10b. The shock wave generated by the expanding channel separated from the channel at $\sim$20 μs and by $\sim$100 μs can be clearly seen at a radius of $\sim$4.5 cm.

v. Comparison of Hydrocode Simulations and Experimental Density Profiles

The evolution of the channel density profile was simulated using the NRL ETBFCT hydrocode.[2] This is a 1-D (radial) Eulerian code which incorporates real gas equilibrium thermodynamics and correctly models shock propagation and heating. In the simulation, energy was deposited instantaneously at time zero by initiating the run with a pressure profile in the form of a "Super-Gaussian" given by

$$p(r,\ t = 0) = p_0 + (p_1 - p_0)\ e^{-\left[\frac{r}{a}\right]^n},$$

where $p(r,\ t = 0)$ is the pressure at radius r for time $t = 0$, p_0 is the ambient gas pressure, p_1 is the pressure on axis ($r = 0$) at $t = 0$, a is the characteristic radius within which the laser energy was deposited, and $n \geqslant 2$. The evolution of the profile was then followed in time until a stable, ambient pressure channel had formed and the outward going shock was some distance from the channel ($\sim$30 μs). The measured value for the energy deposition radius was used as the characteristic radius in conjunction with various different values of deposited energy and a relatively square deposition profile ($n = 5.5$) to achieve a best fit to the measured density profiles. The amount of energy deposited that gave the best fit was then compared to the measured value. This approach was adopted because the initial radius and final profile were considered more accurate measurements than the energy deposited. Flat topped profiles were assumed in accordance with the absorption theory and the dynamic effects discussed below.

The schlieren and interferometric measurements of the stable, ambient pressure, density profiles agree within the expected uncertainties. Figure 11 shows experimental measurements by both methods

for $\sim 100\ \mu s$ after the CO_2 laser pulse. The shock wave was beyond the field of view in each case so the "outside" densities have arbitrarily been set to align with the wings of the simulation which is also plotted on Fig. 11. While the simulation is for $\sim 30\ \mu s$ after the CO_2 laser pulse, the channel profile has stabilized by that time and should be comparable to the results at $\sim 100\ \mu s$. The discrepancy in times does however preclude any comparison of shock wave position and jump conditions. The best match of the channel width and the slope of the channel sides occurs for an assumed energy input of 0.14 J/cm which compares reasonably well with the measured value of .1 J/cm.

Simulations using both smooth (Bennett and Gaussian) and squared (super-gaussian with $2 < n < 10$) profiles have shown that smooth profiles give channels with long sloping sides while squared profiles lead to steep sided, box-like channels. The discrepancy between the measured and predicted values of the on axis density most likely results from a slight deviation of the channel from the circular cross-section assumed to invert the data.

Another dynamic effect is associated with the energy deposition profile. Square deposition profiles cause the on axis channel density to overshoot the stable value and "ring" before reaching an equilibrium value whereas with smooth deposition profiles the central density falls monotonicly to the stable value. Figure 12 compares experimental measurements of the central channel density made with the holographic system to simulations for a square initial heating profile. Both data show the ringing effect. Thus an indirect confirmation exists that the absorption process saturates leading to a flat-topped heating profile.

IV. CHANNEL DECAY

i. Qualitative Observations

Experiments involving single channels, created by heating pulses with both round and oval cross-section, and experiments with compound channels, created by two parallel but spatially and/or temporally offset heating pulses, gave similar results. All channels acquired a fluted appearance (Fig. 13) between 300 μs and 1 ms after formation. This was followed by the appearance of a 3-D turbulent structure. These changes were accompanied by growth in the apparent channel size, i.e. the channel envelope. This growth must have been the result of convective mixing between the cold outside gas and the hot channel since pressure equilibrium had long since been established. We interpret the fluted appearance as a large size 2-D convective flow which subsequently broke up through Kelvin-Helmholtz instability into the 3-D turbulence later observed. The causes of these convective flows have been studied theoretically by Boris and Picone[3] and are predicted to be asymmetries in the channel heating.

ii. Review of Theory

The vorticity of a fluid is defined as the curl of its velocity

$$\omega \equiv \nabla \times \mathbf{v}$$

and is a measure of the amount of rotary motion present in the flow. The equation of motion may be modified (chiefly by taking its curl) into the vorticity equation which shows that crossed pressure and density gradients can change the vorticity within the fluid

$$\frac{\partial \omega}{\partial t} = \frac{1}{\rho^2} (\nabla p \times \nabla \rho) + \text{other terms.}$$

This phenomena causes circulating flows to arise in asymmetrically heated channels and occurs principally when the pressure gradients associated with shocks become misaligned with density gradients. Residual vorticity is left in the fluid at late times after pressure equilibrium has been achieved.

A specific example which was treated in detail by Boris and Picone[3] is shown in Figure 14a. A second, circular heating pulse occurs offset from an existing reduced density channel. The simulations of this situation run by Boris and Picone show that the residual vorticity left after the shock wave from the second pulse has crossed the density gradient of the existing channel takes the approximate form of two vortex filaments (Fig. .14b). Shear exists within this flow and the high Reynolds number ($v \sim c_s/10$, $R_e \sim 10^4$) leads to Kelvin-Helmholtz instabilities. There will result 2-D eddy structures giving the channel a fluted appearance and eventually a chaotic 3-D structure (Fig. 14c).

Integrating the residual vorticity over the half plane on either side of the symmetry axis joining the two channels yields a single number, the vorticity strength, which characterizes the strength of the circulating flows. The vorticity strength is proportional to a form factor which depends on the dimensionless offset between the pulses. A typical curve for this form factor is shown in Fig. 15.

Other asymmetric configurations which have been simulated and lead to convective flows include noncircular heating pulses and two simultaneous but offset heating pulses. These configurations have all been observed experimentally to become turbulent. In addition the structure present in the heating pulses used to create the nominally circular single channels causes even those channels to be turbulent (Fig. 9).

iii. Experimental Results

The effect of two circular heating pulses offset both temporally and spatially was reproduced experimentally by using two $\sim$50 J CO_2 laser pulses separated by $\sim$100 μs and brought through the NaCl focusing lens at different positions and angles to give approximately parallel channels near focus. Experiments were run at dimensionless offsets (as indicated by burn patterns) of 1.4 and 2.8 (Fig. 16). These experiments were observed using the Mach-Zehnder interferometer, high speed camera combination. Selected frames from these movies (and a movie of a single round channel) are shown in Fig. 13. The large scale flow (2 vortex filaments) predicted by theory is disrupted before becoming evident in these photographs and we first observe more complicated 2-D (fluted) structures and eventually 3-D turbulence. The level of turbulence appears to be greater for the lesser offset which is consistent with the dependancy of the form factor. The turbulence is least for the single round channel with its lesser asymmetries.

In similar experiments two side by side oval channels were produced simultaneously and observed both from the side and above with the schlieren system coupled to the high speed camera. This case is similar to that of two simultaneously produced round channels which was studied theoretically. The simulations predicted four vortex filaments positioned to pump gas out from between the channels. Figure 17 shows the top and side views of this experiment. It is evident from the side view that gas was being expelled from between the channels whereas in the top view very little spreading occurs. In Fig. 18 the average radius versus time is plotted for both views and this directional effect is again evident. Thus evidence exists in this experiment of the large scale flows predicted by theory. In time this flow also disrupted and the composite channel became turbulent.

iv. Late Time Behavior, Turbulent Diffusion

Even for the single round channels large scale convective flows disrupted in time to give the turbulent behavior noted in the movies. These channels also continued to grow showing that mixing continued between the cold outside air and the hot channel. We have applied simple turbulence theory to predict the scaling with time of this growth.[11] A brief review of this work follows. As the eddy cells shuffle parcels of gas about in a random manner the average effect is like an anomalous diffusion of both matter and heat. Given a characteristic eddy cell size l, and a characteristic eddy velocity v the anomalous diffusivity is $\alpha = lv$. The governing equations of fluid motion may be averaged in such a way that the effect of turbulence appears as an (anomalous) diffusive term in each equation. Based on these equations the scaling with time is found to be

$$r^2(t) = r^2(\tau) + 4\alpha(t - \tau)$$

where $r(t)$ is the channel radius at time t and $r(\tau)$ the radius at $t = \tau$. A self-similar expansion of a Gaussian profile is assumed and leads to the numerical factor of 4.

The average radius of the turbulent round channel was measured, as a function of time, from the interferometric movies. The square of this radius is plotted versus time in Fig. 19. This plot shows two linear regions. Up to $\sim$500 μs (Fig. 19a) a more rapid growth corresponding to an anomalous diffusivity of $\sim$250 cm^2/sec occurred and corresponds to the period when 2-D fluting was apparent. Beyond that time (Fig. 19b) the channel showed 3-D turbulence and displayed diffusive growth at a rate of $\sim$60 cm^2/sec. The rate of growth declined steadily after the first 20 ms such that the average over the total observation time of 60 ms was $\alpha \sim 30$ cm^2/s. Beyond $\sim$60 ms the edges of the channel were not clearly enough defined to measure a radius. Such anomalous diffusivity greatly exceeds the true thermal diffusivity of $\sim$.2 cm^2/s so channel dissipation is greatly enhanced by the turbulence.

V. CONCLUSIONS

Our experimental chamber has functioned as intended, in particular the windowless transition region successfully separated the clean and doped nitrogen flows. The SF_6 detection system was a sensitive monitor of the cleanliness of the nitrogen gas in the convergence section.

The general description of the absorption process for 10.6 μ radiation by the SF_6 gas appears to fit the experimental absorption measurements. The absorption appears to have saturated at approximately the calculated value, and the details of the density profile measurements also indicate a saturation effect.

Reasonable agreement exists between the observed evolution of the density profile, the measured initial conditions, and the hydrocode simulations of the channel formation process.

All channels observed dissipated by turbulent mixing at rates greatly exceeding that predicted by thermal diffusion. Thus these results follow the general pattern of channel cooling by turbulent mixing seen in channels produced by electric discharges in the atmosphere,[5] and further support the hypothesis that hot channels in the atmosphere, produced by lightning, will also cool much more rapidly ($\sim$ 100 to 1000 times faster) than simple thermal conduction. In experiments intended to test the vorticity theory of Boris and Picone[3] concerning the source of this turbulence, qualitative support was found for the dependancy of the strength of the turbulence on the dimensionless spatial offset between time staggered heating pulses. Experiments with simultaneous offset channels also gave qualitative evidence for the existence of the large scale convective flows predicted by the theory.

The dissipation of the channels occurs as the result of turbulent mixing and fits well to a diffusive model of the process.

VI. ACKNOWLEDGMENT

The authors note, once again, their gratitude for the technical support provided by Mr. E. Laikin throughout this experiment. They also thank their colleagues Drs. M. Lampe and S. Kainer who provided results from their theoretical studies of channel formation; Drs. J. P. Boris and J. M. Picone who developed the theory and numerical simulations of channel decay, and provided results for comparison with the experiment; and Dr. A. W. Ali who provided information and understanding regarding the structure of SF_6 and the mechanisms of energy transfer.

This work has been supported by the Office of Naval Research and the Defense Advanced Research Projects Agency.

VII. REFERENCES

1. R.E. Pechacek, J.R. Greig, M. Raleigh, and S.R. Rod, NRL Memorandum Report 3602 (1977).

2. M. Lampe and S. Kainer, NRL Memorandum Report 4129 (1979).

3. J.P. Boris and J.M. Picone, NRL Memorandum Report 4327 (1980).

4. R.D. Hill, R.G. Rinker, and H.D. Wilson, J. Atmos. Sci. **37**, 179-192 (1980).

5. J.M. Picone, J.P. Boris, J.R. Greig, M. Raleigh, and R.F. Fernsler, J. Atmos. Sci. **38**, 2056-62 (1981); [see also NRL Memorandum Report 4380 (1981)].

6. A.V. Nowak and J.L. Lyman, J. Quant. Spectrosc. Radiat. Transfer **15**, 945-961 (1975).

7. S.A. Akhmanov, V.M. Gordienko, A.V. Mikheenko and V.Ya. Panchenko, JETP Lett. **26**, 453-456 (1977).

8. M. Raleigh and J.R. Greig, NRL Memorandum Report 4390 (1981).

9. F.C. Jahoda and R.E. Siemon, Los Alamos Scientific Laboratory Informal Report, LA-5058-MS, VC-37 (1972).

10. J.G. Black, E. Yablonovitch, N. Bloembergen, and S. Mukamel, Phys. Rev. Lett. **38**, 1131-4 (1977).

11. M. Raleigh, NRL Memorandum Report 4555 (1981).

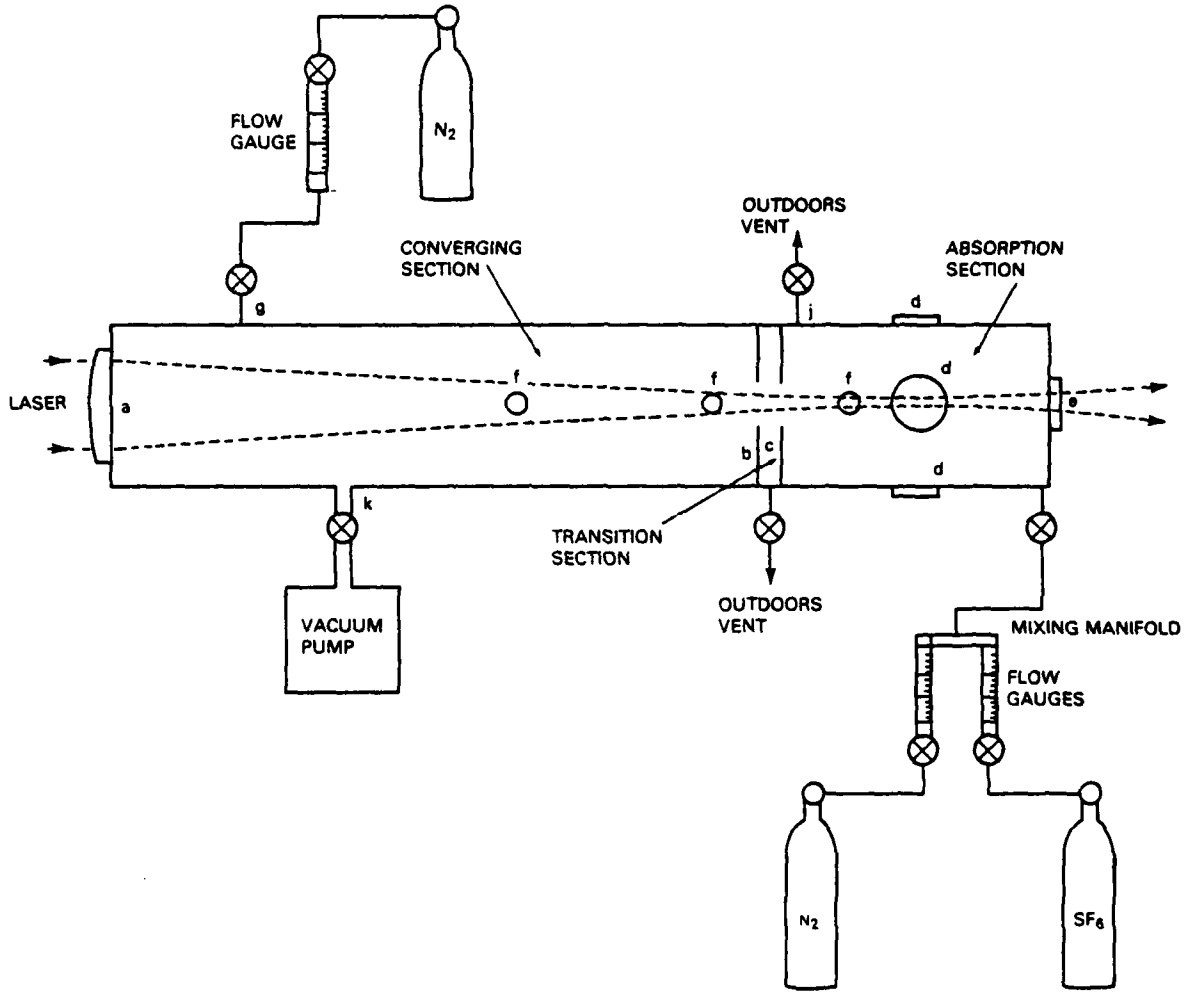

Fig. 1 — A side view of the experimental chamber showing the gas flow system and the diagnostic windows and ports. The approximate CO_2 laser beam envelope is indicated by dashed lines.

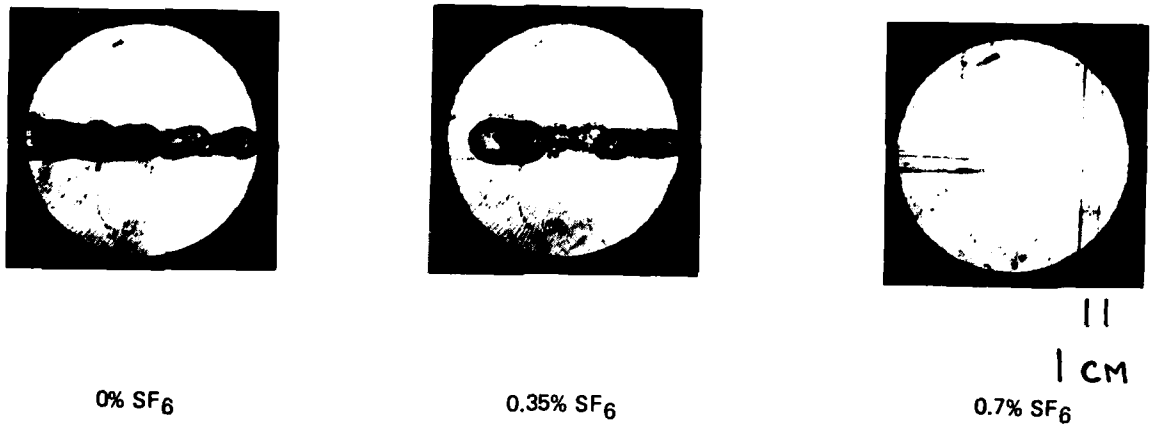

Fig. 2 — Schlieren photographs showing channels produced by the absorption of 10.6 μm radiation in N_2 doped with various amounts of SF_6. All photographs are 25 ns exposures taken 4 μs after the CO_2 laser pulse. A 1 mm pinhole was used in place of the usual knife edge to reveal both vertical and horizontal density gradients. The view is through the 15 cm windows in the absorption section and the CO_2 laser was incident from the left.

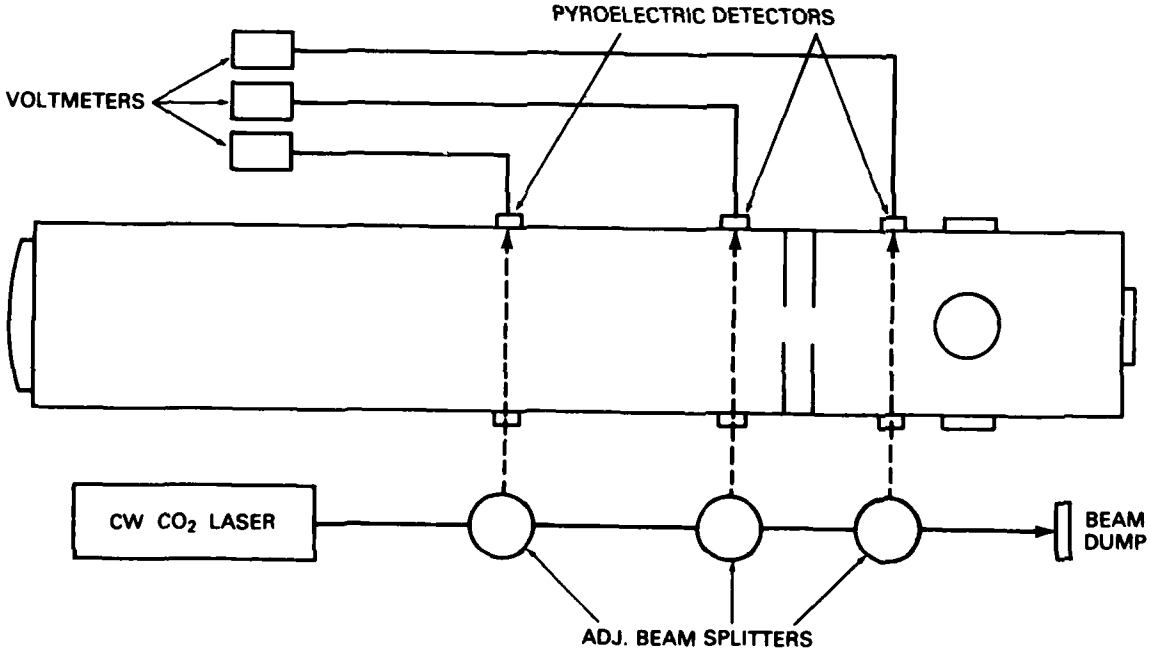

Fig. 3 — A top view of the experimental chamber showing the SF_6 monitoring system.

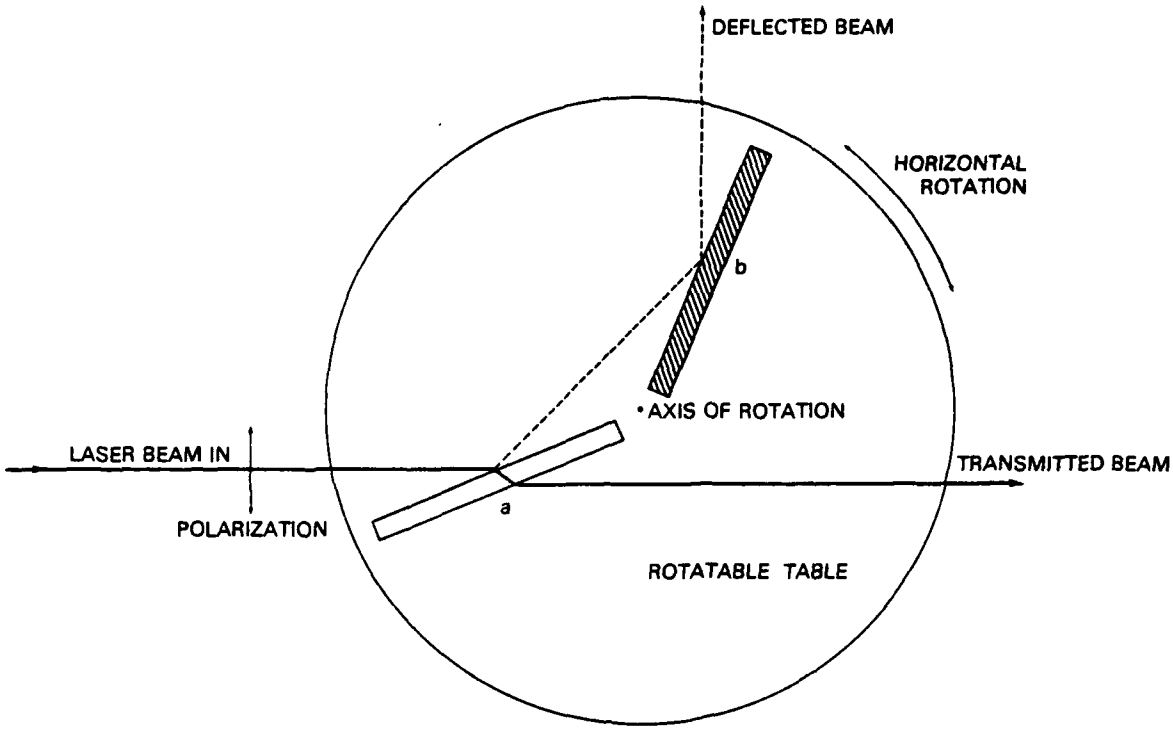

Fig. 4 — The adjustable beam splitter used in the SF_6 monitoring system.

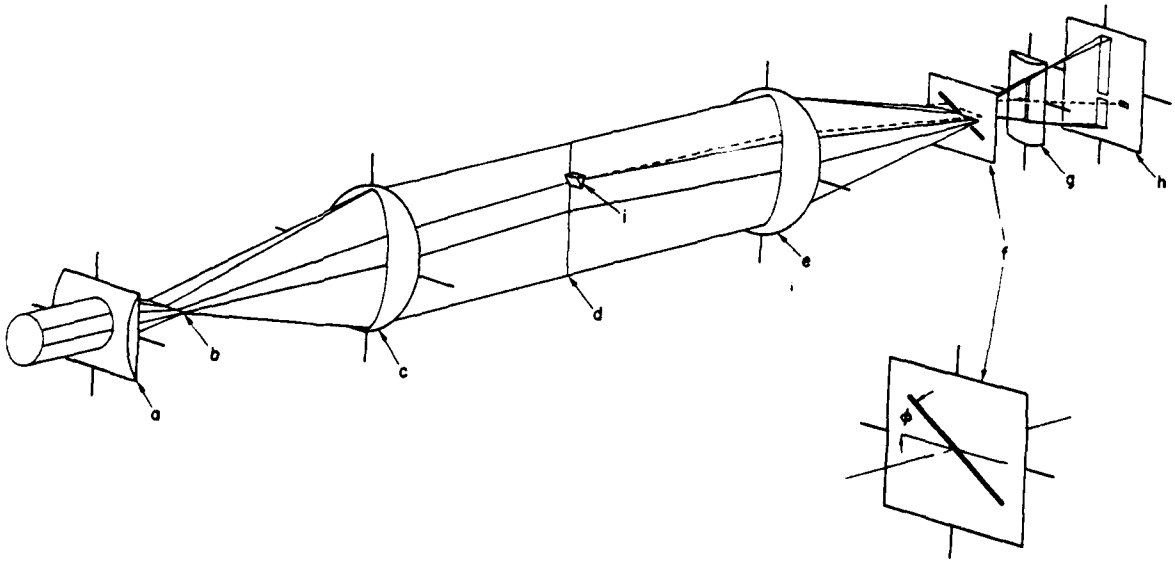

Fig. 5 — The optical train of the quantitative schlieren system.

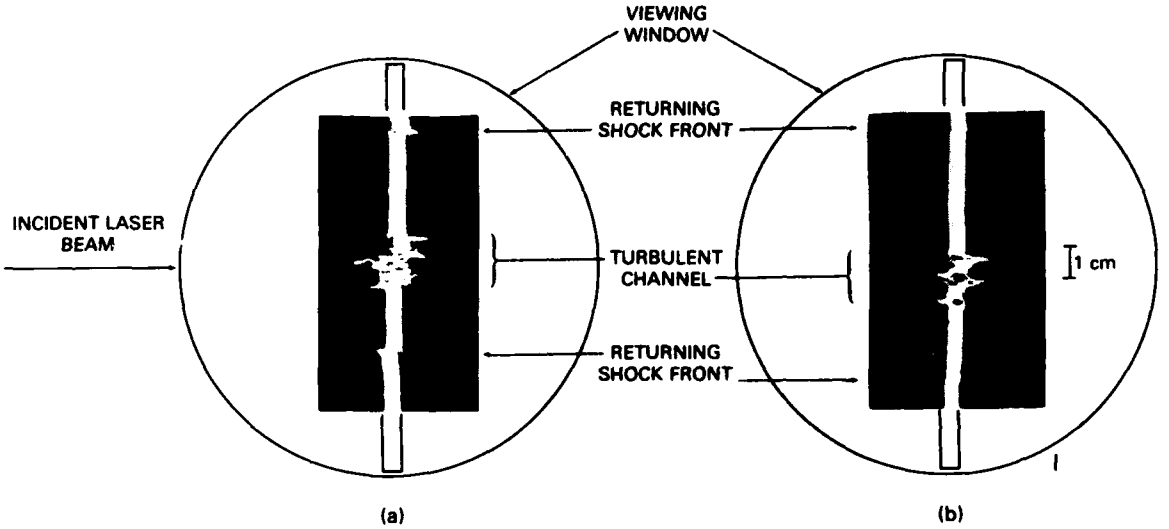

Fig. 6 — Quantitative schlieren photographs showing the attenuation of the returning shock wave after carpeting the interior of the chamber. Both photographs are 25 ns exposures taken 800 μs after the CO_2 laser pulse (a) without carpet, (b) with carpet.

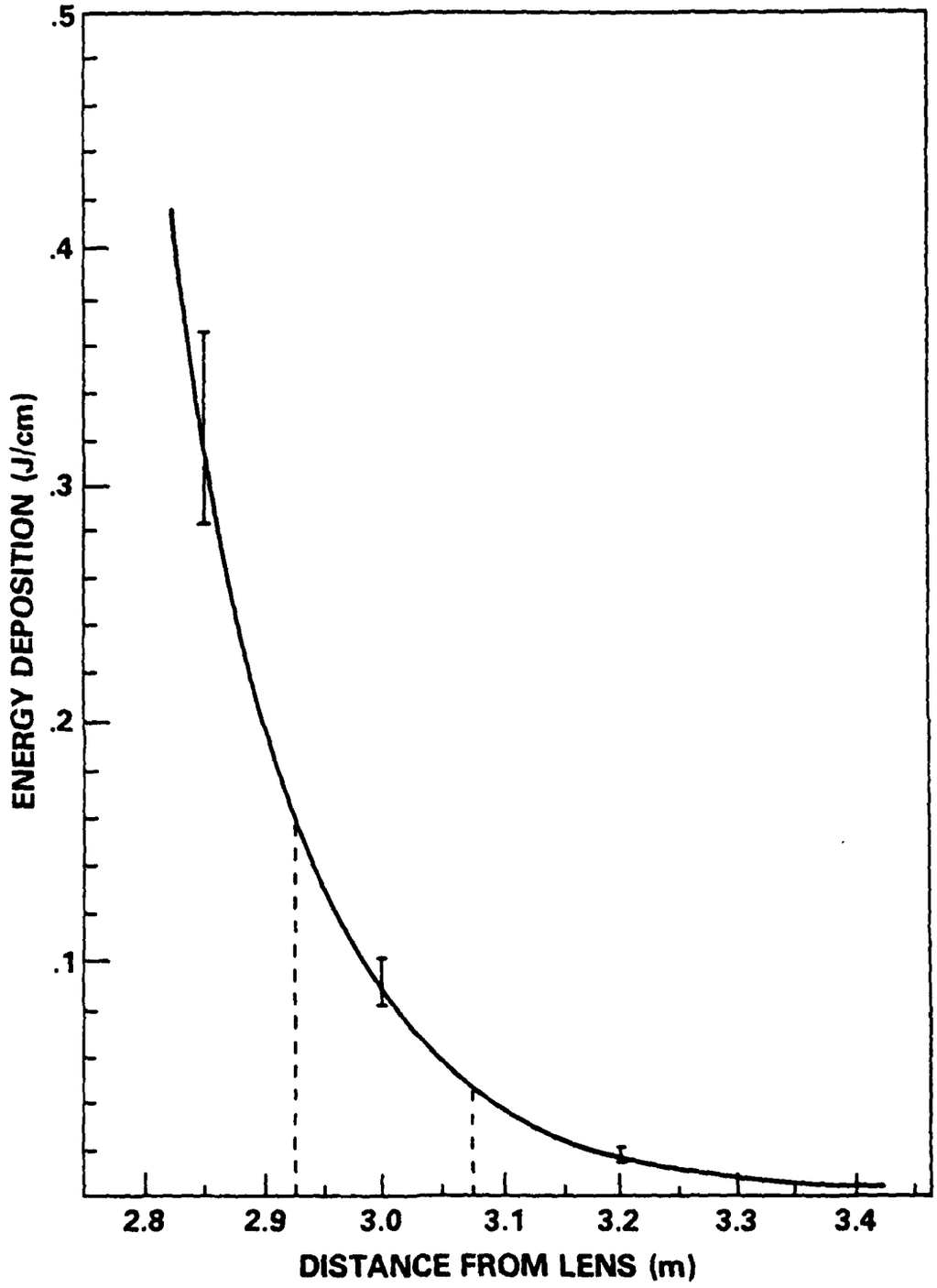

Fig. 7 — A graph showing the laser energy absorbed per centimeter of channel length for a round beam, versus distance from the lens. The field of view is noted by the dashed lines. The data was measured with a calorimeter under actual gas flow conditions.

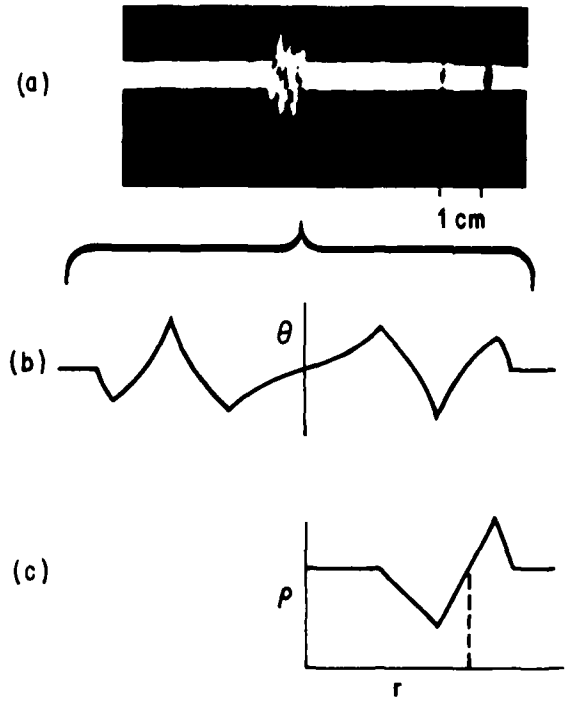

Fig. 8 — A quantitative schlieren photograph (a) of the channel at $t = 2\ \mu s$. While the photograph has not been inverted, the general features, shown expanded in (b), may be interpreted as resulting from an outward going shock and an inward going rarefaction as shown in (c).

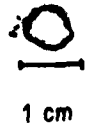

Fig. 9 — A burn pattern for a single round beam taken at the center of the field of view and showing the irregularities present in this laser pulse.

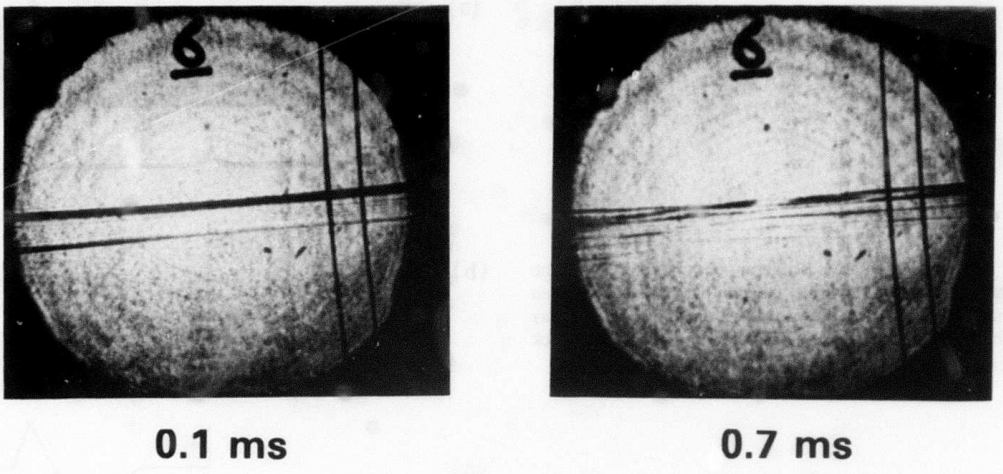

Fig. 10 — (a) Schlieren photographs of a single round channel. The time of the exposure after the CO_2 laser pulse is quoted in μs beneath each photograph. The transition from a uniform channel through 2-D to 3-D disturbances is seen.

10μs

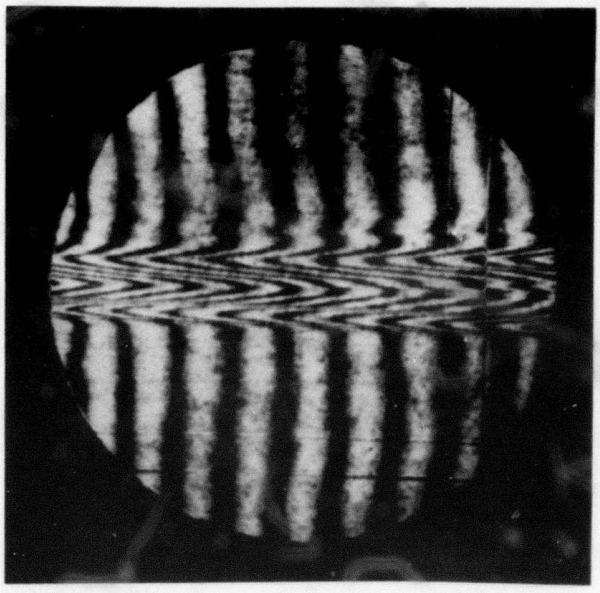

100μs

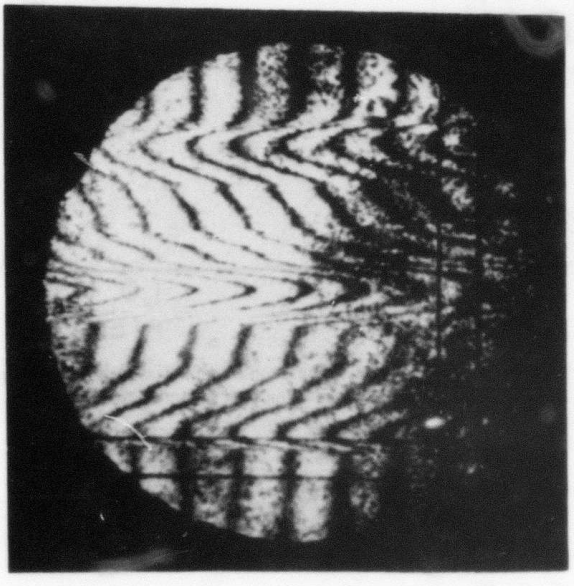

Fig. 10 — (b) Interferograms of the single round channel at 10 μs and 100 μs after the CO_2 laser pulse.

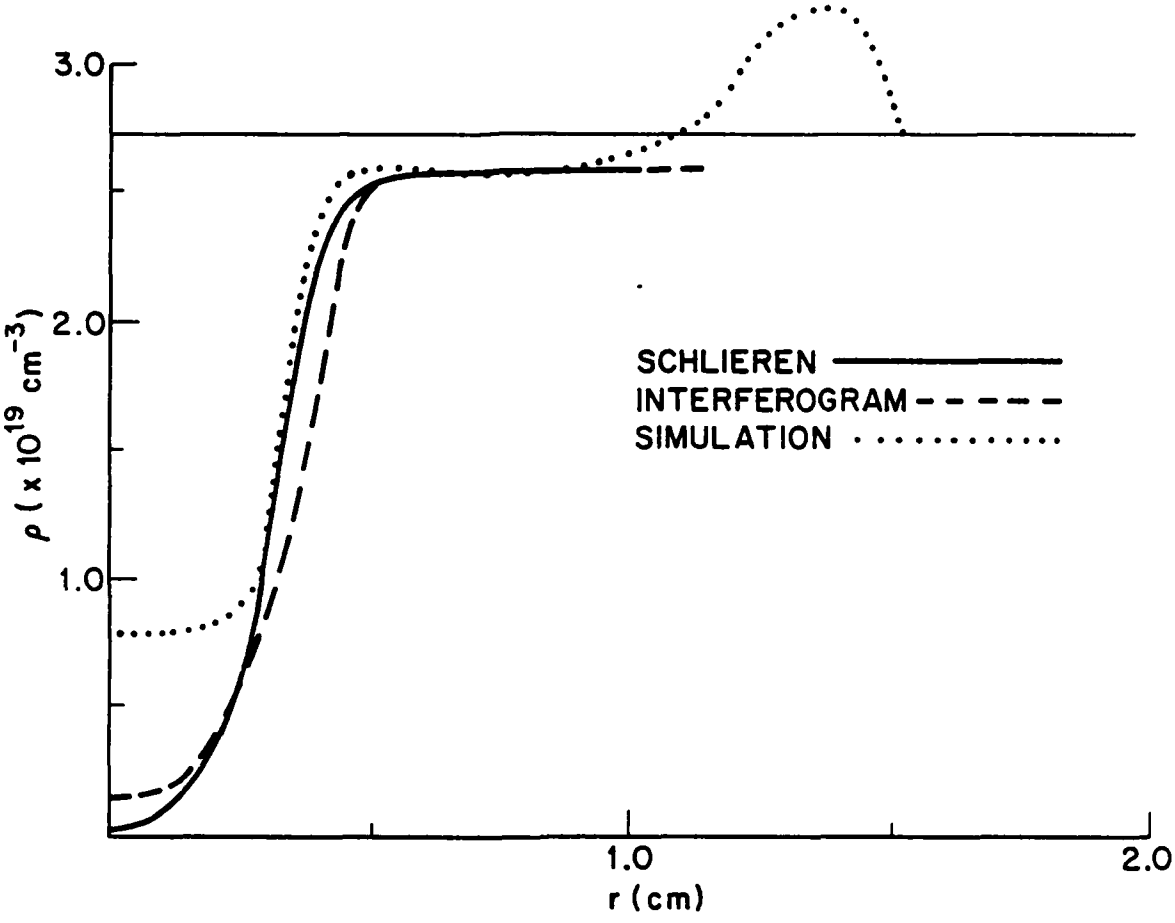

Fig. 11 — The radial density profile of the single round channel at ~100 μs as measured with both the Mach-Zehnder interferometer and the quantitative schlieren systems. The best fit simulation is also shown but is for a time of ~30 μs and therefore still shows the shock wave. In the simulation $n = 5.5$.

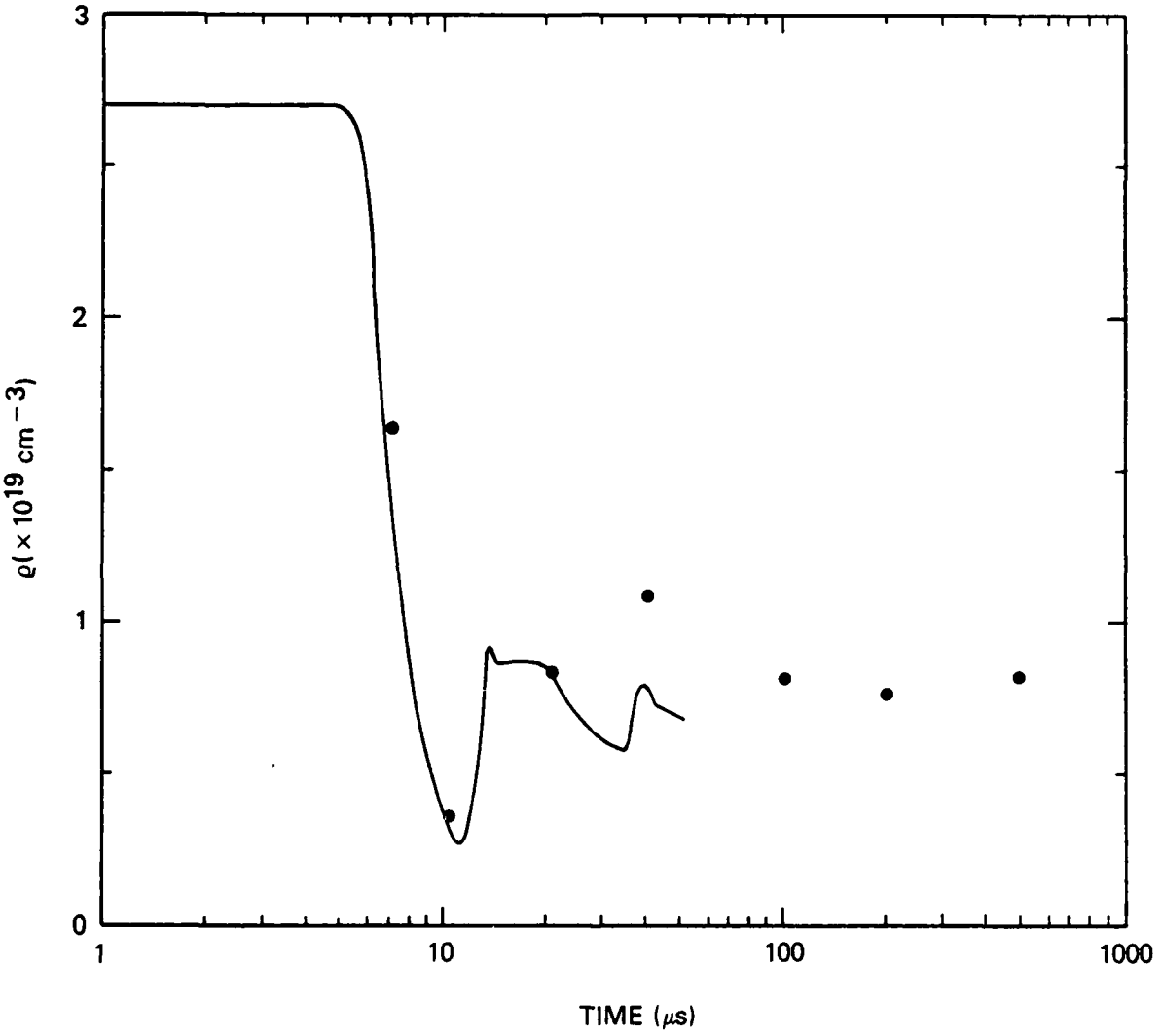

Fig. 12 — The on-axis channel density versus time as measured by holographic interferometry (·). Also shown are calculated densities from the simulation (—). Both show the density to undershoot the pressure equilibrium value and oscillate before stabilizing.

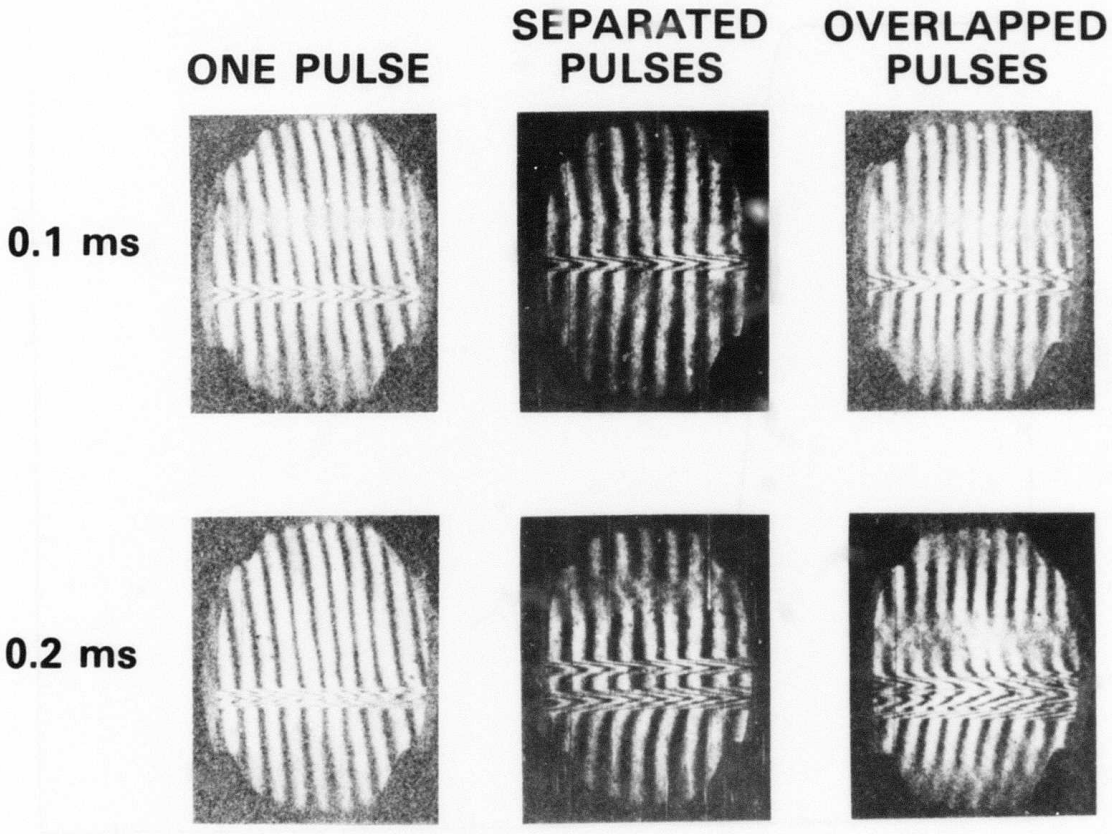

Fig. 13 — Individual frames from the interferometric movies for a singly pulsed channel and for doubly pulsed channels at two different offsets. In the doubly pulsed case, the two laser pulses were 100 μs apart.

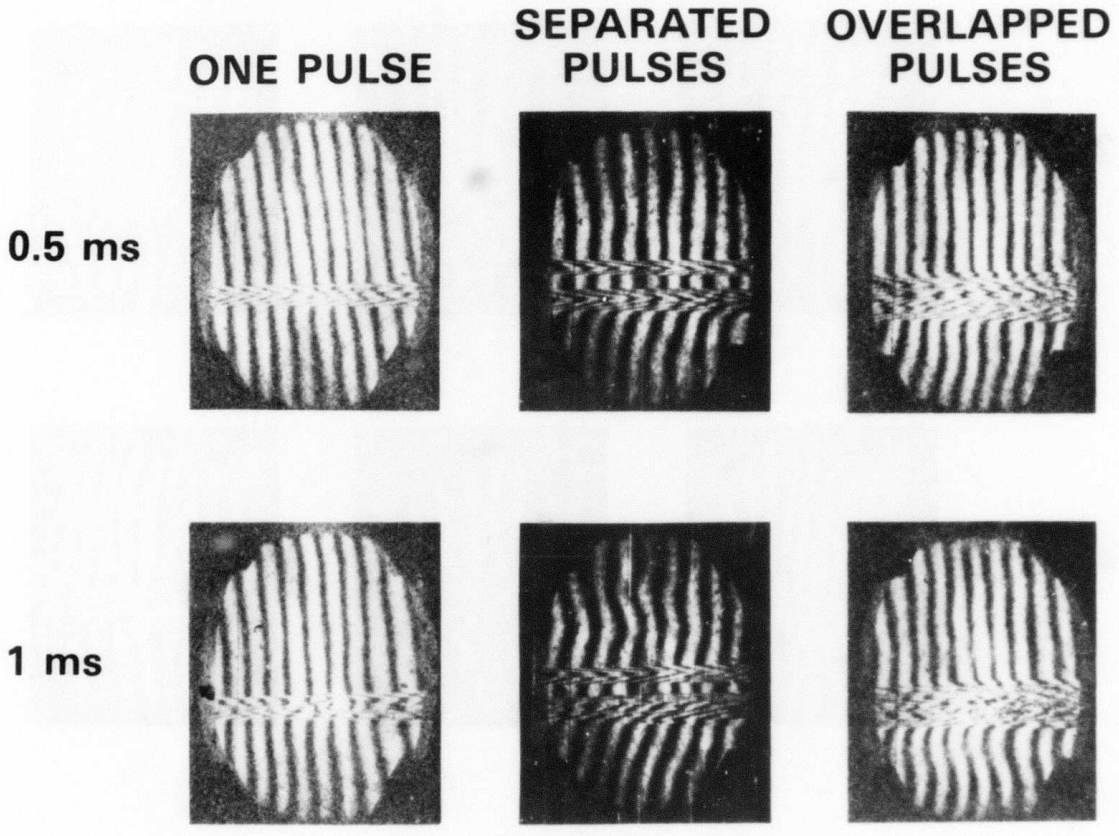

Fig. 13 (Continued) — Individual frames from the interferometric movies for a singly pulsed channel and for doubly pulsed channels at two different offsets. In the doubly pulsed case, the two laser pulses were 100 μs apart.

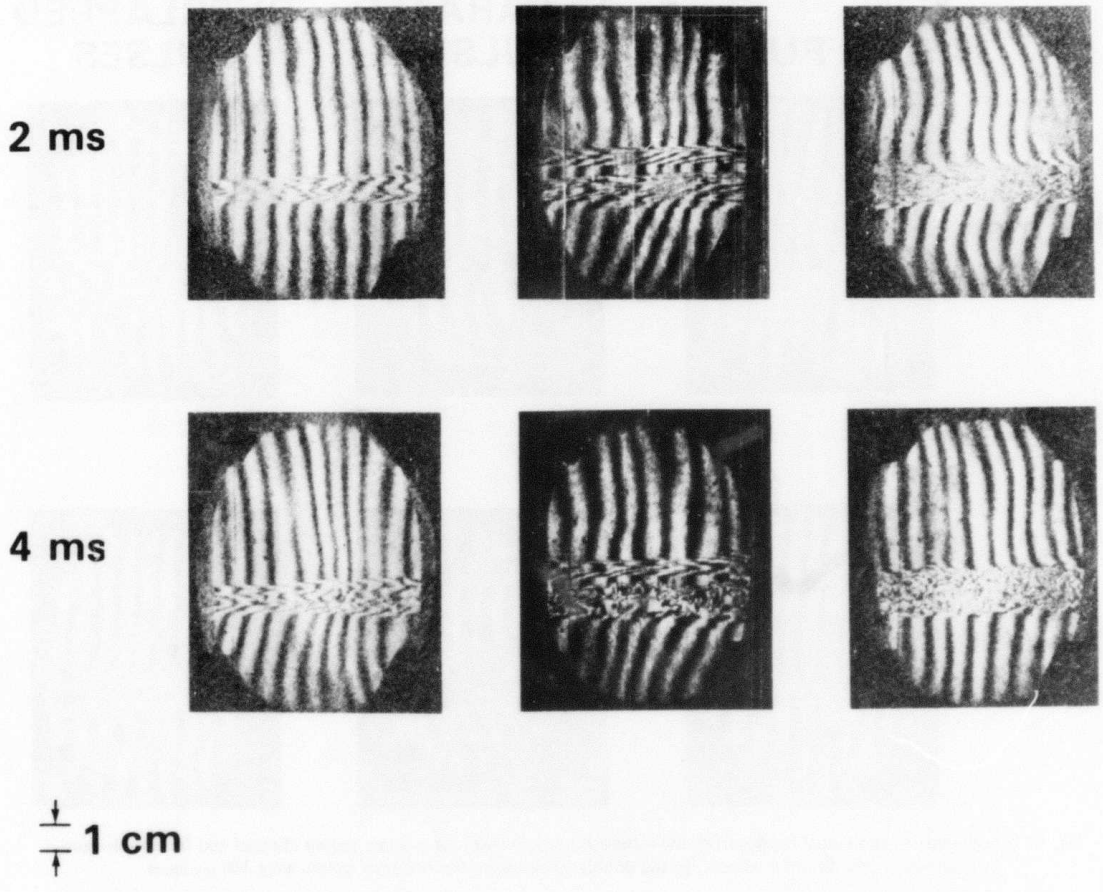

Fig. 13 (Continued) — Individual frames from the interferometric movies for a singly pulsed channel and for doubly pulsed channels at two different offsets. In the doubly pulsed case, the two laser pulses were 100 μs apart.

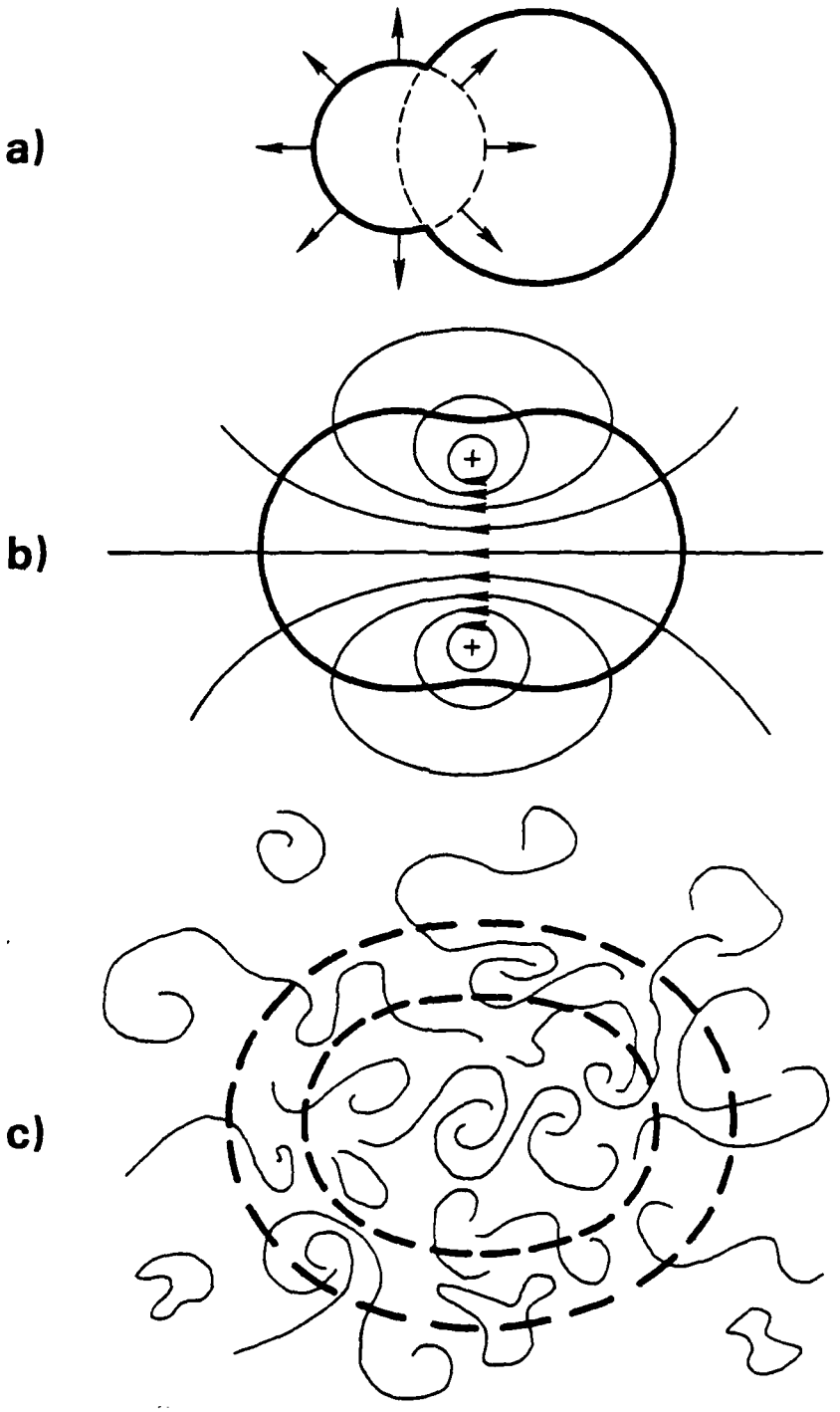

Fig. 14 — An example of the generation of vorticity and turbulence by heating asymmetries. (a) A second heating pulse deposits energy off-axis from an existing channel. (b) The hypothetical velocity distribution left, after pressure equilibrium is achieved, is approximately two vortex filaments as shown. (c) The high Reynolds number causes this flow to be unstable. A 2-D pseudo turbulence develops before any substantial fluid drift occurs and the channel assumes a fluted appearance. This flow then degenerates into a true 3-D turbulence and the channel appears rumpled.

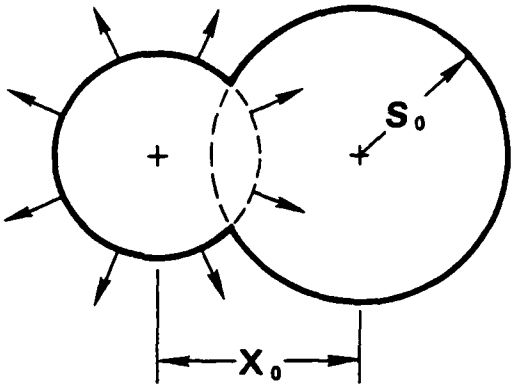

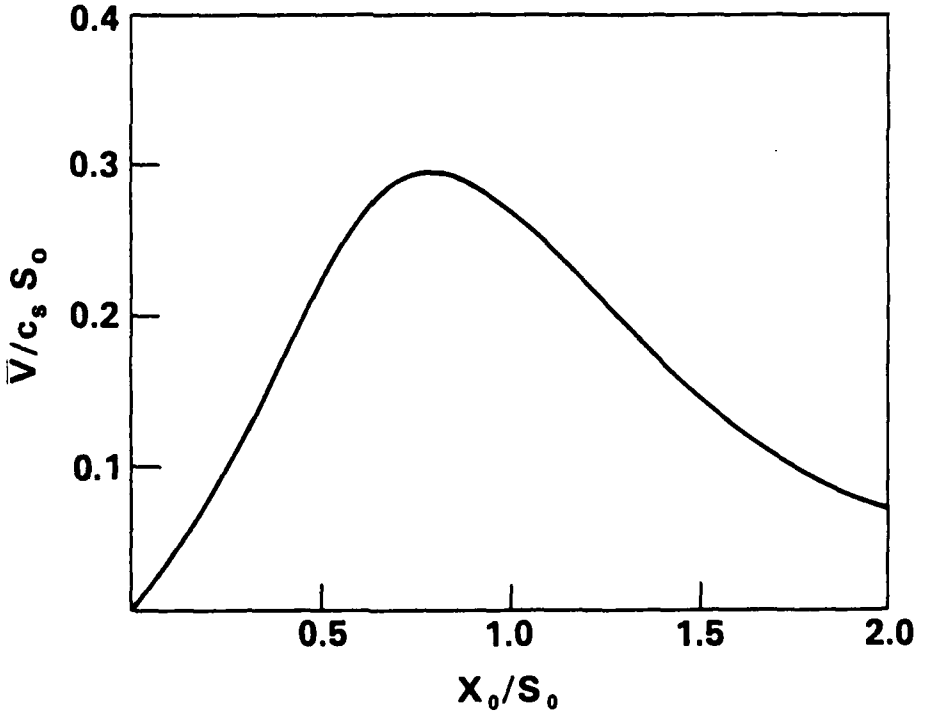

Fig. 15 — The dimensionless vorticity strength versus the dimensionless offset for Bennett profile heating pulses (c_s = sound speed) taken from Boris and Picone[3]. Similar form factors result for Gaussian and square heating pulses.

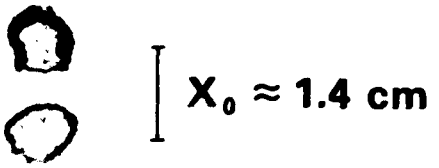

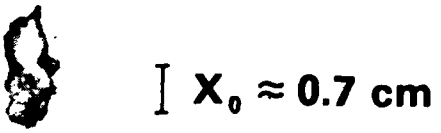

Fig. 16 — Laser burn patterns taken at focus for two different spatial separations. In both cases the equilibrium size of the first channel, S_0, is $\sim .5$ cm so dimensionless separations of ~ 1.4 and ~ 2.8 are represented by these shots.

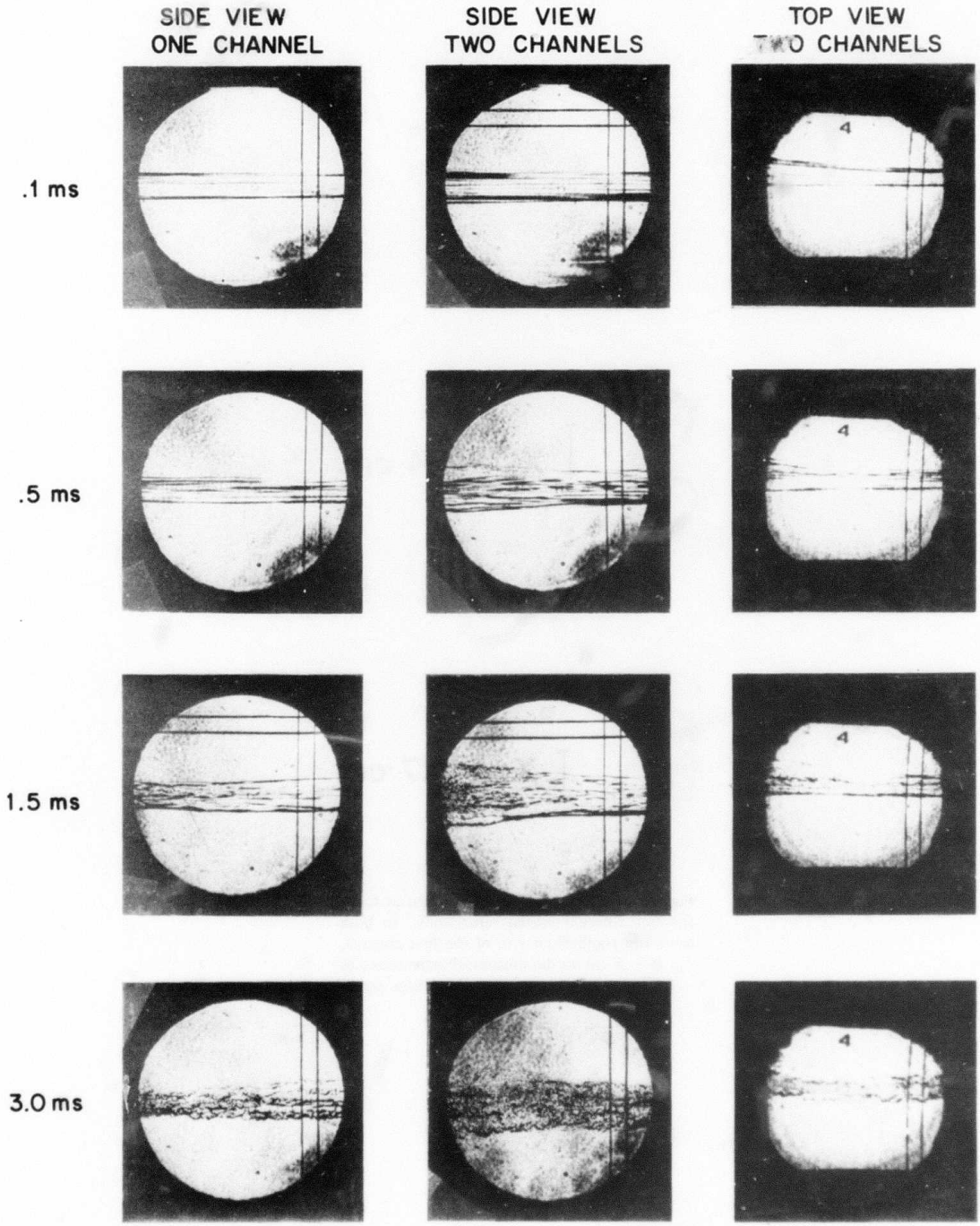

Fig. 17 — Schlieren photographs of two oval channels which are spatially offset but produced simultaneously. The expulsion of gas from between the channels is evident in the side view.

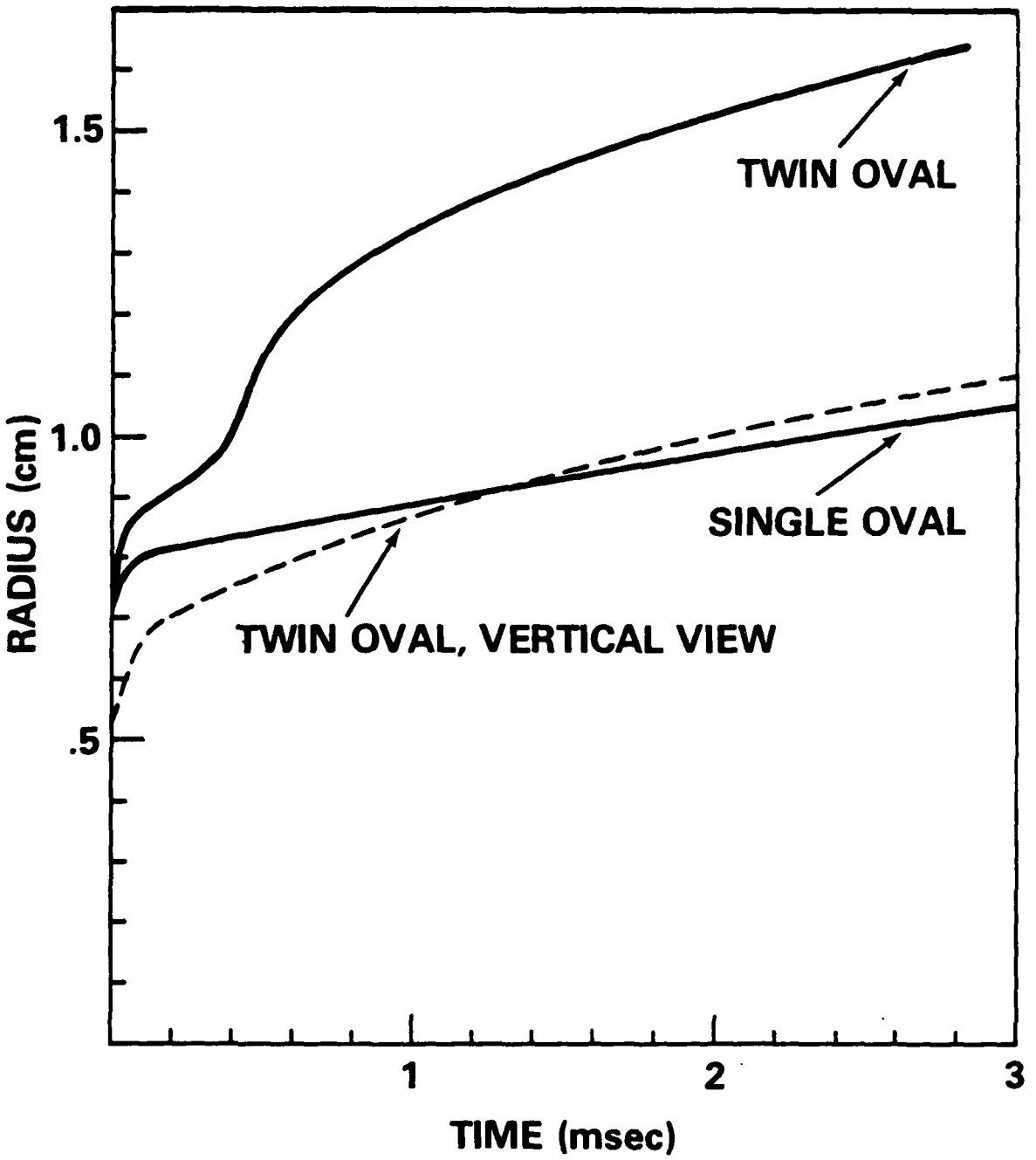

Fig. 18 — The average radius versus time for both side and top views of the simultaneous oval channels. The expulsion of gas is evident in the side view.

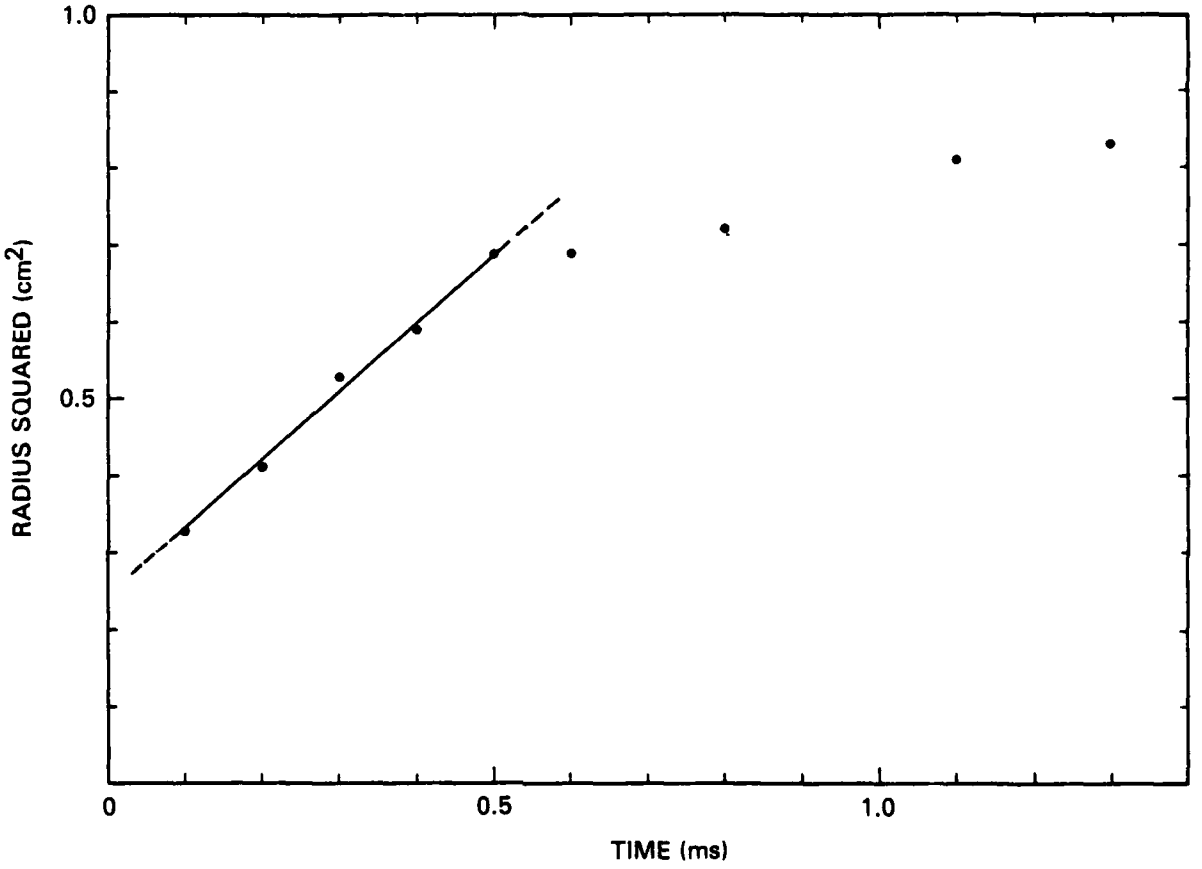

Fig. 19 — The square of the average channel radius versus time for a single round channel.
(a) viewed for the first few milliseconds only.

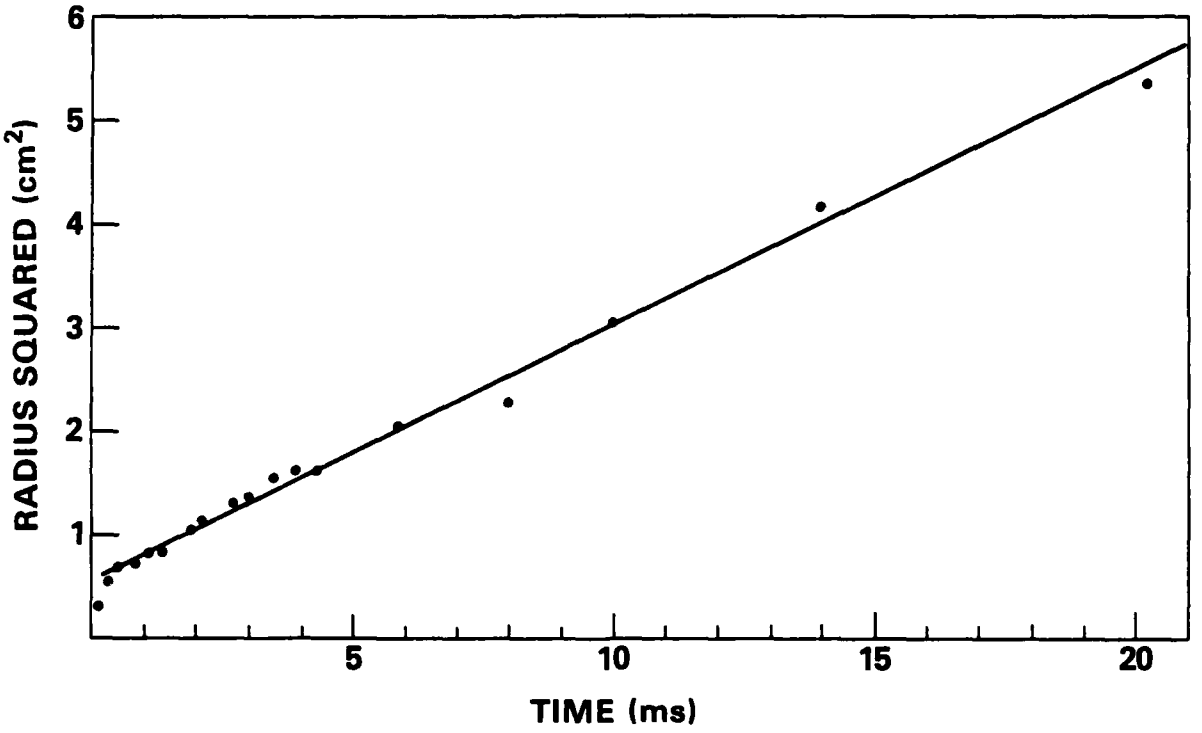

Fig. 19 — The square of the average channel radius versus time for a single round channel. (b) viewed over longer times.